Light bullets in a time-delay model of a wide-aperture mode-locked semiconductor laser

Article *in* Philosophical Transactions of The Royal Society A Mathematical Physical and Engineering Sciences · July 2018

DOI: 10.1098/rsta.2017.0372

4 authors:

Alexander Pimenov
Weierstrass Institute for Applied Analysis and Stochastics
57 PUBLICATIONS **343** CITATIONS
SEE PROFILE

Julien Javaloyes
University of the Balearic Islands
174 PUBLICATIONS **1,464** CITATIONS
SEE PROFILE

Svetlana V. Gurevich
University of Münster
82 PUBLICATIONS **625** CITATIONS
SEE PROFILE

A. G. Vladimirov
Weierstrass Institute for Applied Analysis and Stochastics
136 PUBLICATIONS **2,024** CITATIONS
SEE PROFILE

PHILOSOPHICAL TRANSACTIONS A

rsta.royalsocietypublishing.org

Research

Cite this article: Pimenov A, Javaloyes J, Gurevich SV, Vladimirov AG. 2018 Light bullets in a time-delay model of a wide-aperture mode-locked semiconductor laser. *Phil. Trans. R. Soc. A* **376**: 20170372.
http://dx.doi.org/10.1098/rsta.2017.0372

Accepted: 24 April 2018

One contribution of 11 to a theme issue 'Dissipative structures in matter out of equilibrium: from chemistry, photonics and biology (part 1)'.

Subject Areas:
optics

Keywords:
light bullets, wide-aperture laser, mode-locking, time-delay model

Author for correspondence:
A. G. Vladimirov
e-mail: vladimir@wias-berlin.de

Light bullets in a time-delay model of a wide-aperture mode-locked semiconductor laser

A. Pimenov[1], J. Javaloyes[2], S. V. Gurevich[3,4] and A. G. Vladimirov[1,5]

[1]Weierstrass Institute, Mohrenstrasse 39, 10117 Berlin, Germany
[2]Departament de Física, Universitat de les Illes Balears, C/ Valldemossa km 7.5, 07122 Mallorca, Spain
[3]Institute for Theoretical Physics, University of Münster, Wilhelm-Klemm-Strasse 9, 48149 Münster, Germany
[4]Center for Nonlinear Science (CeNoS), University of Münster, Corrensstrasse 2, 48149 Münster, Germany
[5]Lobachevsky State University of Nizhni Novgorod, pr. Gagarina 23, Nizhni Novgorod 603950, Russia

AGV, 0000-0002-7540-8380

Recently, a mechanism of formation of light bullets (LBs) in wide-aperture passively mode-locked lasers was proposed. The conditions for existence and stability of these bullets, found in the long cavity limit, were studied theoretically under the mean field (MF) approximation using a Haus-type model equation. In this paper, we relax the MF approximation and study LB formation in a model of a wide-aperture three section laser with a long diffractive section and short absorber and gain sections. To this end, we derive a non-local delay-differential equation (NDDE) model and demonstrate by means of numerical simulations that this model supports stable LBs. We observe that the predictions about the regions of existence and stability of the LBs made previously using MF laser models agree well with the results obtained using the NDDE model. Moreover, we demonstrate that the general conclusions based upon the Haus model that regard the robustness of the LBs remain true in the NDDE model valid beyond the MF approximation, when the gain, losses and diffraction per cavity round trip are not small perturbations anymore.

THE ROYAL SOCIETY PUBLISHING

This article is part of the theme issue 'Dissipative structures in matter out of equilibrium: from chemistry, photonics and biology (part 1)'.

1. Introduction

The formation of nonlinear localized structures (LSs) has been the subject of substantial interest over recent decades. The concept of dissipative LSs is based on three main foundations: classical soliton theory, bifurcation theory and Prigogine's ideas of self-organization [1]. An interesting example of three-dimensional LSs is provided by the so-called 'light bullets' (LBs), pulses of electromagnetic energy that are localized both in space and time and preserve their shape in the course of their propagation. Since the paper of Silberberg [2], who coined the term 'LBs' and demonstrated that the 'naive' conservative Kerr LBs found in the nonlinear Schrödinger equation are unstable and collapse in three dimensions (for more details on the collapse, see [3,4]), experimental observation of LBs remains one of the challenging problems in nonlinear optics. Silberberg showed that the balance between a self-focusing nonlinearity and the spreading effect of chromatic dispersion and/or diffraction was not sufficient to define a robust LB formation scenario. During the last 20 years, other confinement mechanisms were envisioned in different nonlinear optical systems. In particular, LBs were predicted in dissipative systems like, e.g., optical parametric oscillators [5] or bistable cavities [6,7] with an instantaneous response of the active medium, and more recently in the output of a passively mode-locked laser operated in the long cavity regime [8,9]. However, these studies were performed with the help of the Haus-type partial differential equations derived in the mean field (MF) limit when gain and loss per cavity round trip were small and the diffraction was weak, an assumption which is hardly justified for real semiconductor laser devices. Therefore, while the basic mechanism of the formation of the LBs can be qualitatively understood using the models of [8,9], determining the parameter domains where this phenomenon can be observed experimentally requires further theoretical studies. To that end, the understanding of the existence and stability properties of LBs with respect to various laser parameters is crucial for the experimental success, which is ongoing research at the moment.

Unlike the MF laser models, the delay differential equations (DDEs) developed in [10–12] and successfully applied to analyse complex dynamical phenomena in mode-locked lasers [10–14] are free from the small gain and loss approximation. The DDE model describes time evolution of the slowly varying envelope of the electric field in a ring cavity consisting of multiple sections such as gain, absorber and spectral filter under some general physical assumptions about each section [11]. Moreover, DDE laser models were successfully tested over recent years to investigate multi-longitudinal-mode regimes observed in various experimental set-ups [13–19] including the lasers with Fabry–Perot cavities [20–23], which are conventionally studied using more complicated travelling wave partial differential equation models [24–28].

To study the dynamics of a wide aperture mode-locked semiconductor laser, we derive a non-local delay-differential equation (NDDE) model that can be considered as a generalized version of the DDE mode-locking model taking into account the diffraction in the transverse plane. Using this model, we discover for the first time stable LBs in the parameter domain where the MF approximation is no longer valid, and demonstrate that their existence ranges and stability properties are qualitatively similar to those found in [8,9], which confirms the robustness of the LBs. Furthermore, we demonstrate that by using a spectral method optimized for the computation of LBs in a narrow temporal window we can considerably reduce the LB computation cost. We use the spectral functional mapping to study the stability properties of the LBs in transition away from the MF limit, and show that numerical results obtained using this method are in perfect agreement with those obtained by direct numerical integration of the NDDE model. It is noteworthy that following the approach introduced in [29] in the limit of small gain and loss per cavity round trip and weak diffraction one can reduce the described NDDE model to generic partial differential

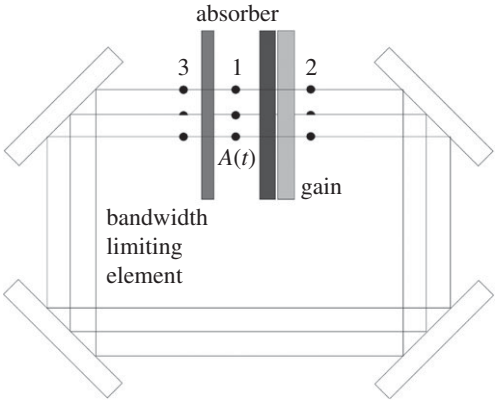

Figure 1. Schematic of a wide-aperture ring external cavity laser with thin absorber, gain and spectral filtering sections. The numbered points 1, 2 and 3 indicate the longitudinal coordinates of the transverse sections where the electric field envelopes A_j with $j = 1, 2, 3$ are evaluated. The output of the laser is taken from one of the cavity mirrors. The relationship between these envelopes are given by equations (2.1)–(2.3).

MF equations of the Haus type where the effects of gain, losses, chromatic dispersion and/or diffraction can be easily incorporated. On the other hand, incorporating chromatic dispersion into the DDE models is not as straightforward. For example, theoretical approaches allowing to extend DDE models of multimode lasers to account for chromatic dispersion of the intracavity media leading to differential equations with distributed time delay were proposed in [15,30,31].

2. Model equations

In this section, we derive a model of a wide-aperture mode-locked semiconductor laser shown schematically in figure 1. Similar to [10–12], we use the lumped element approach, which assumes that gain, absorption, diffraction and spectral filtering are separated and attributed to different laser sections. Therefore, assuming that the absorber and gain sections are very thin and placed one after another, we neglect the diffraction and express the electric field amplitude A_2 on the output of the gain section via the amplitude A_1 on the entrance of the absorber section as

$$A_2(t,x,y) = \mathrm{e}^{(1-\mathrm{i}\alpha_g)G(t,x,y)/2-(1-\mathrm{i}\alpha_q)Q(t,x,y)/2+\mathrm{i}\phi_1} A_1(t-t_1,x,y), \tag{2.1}$$

where t_1 describes small time delay introduced by these two sections, α_g and α_q are linewidth enhancement factors, ϕ_1 is the phase shift, G and Q are the saturable gain and loss proportional to the integrals of the carrier density along the characteristics over the gain and absorber sections, respectively [10–12].

Next, we consider a section where the diffraction takes place. In the Fresnel diffraction approximation, the output field A_3 from this section can be expressed via the input field A_2 as follows:

$$A_3(t,x,y) = \sqrt{\kappa}\frac{\mathrm{e}^{\mathrm{i}kL}}{2\pi\,\mathrm{i}} \iint_{-\infty}^{\infty} \mathrm{e}^{\mathrm{i}[(x-x')^2+(y-y')^2]/2} A_2(t-t_2,x',y')\,\mathrm{d}x'\,\mathrm{d}y', \tag{2.2}$$

where x and y are dimensionless transverse coordinates, L is the section length, $t_2 = L/v$ is the delay time, v is the light velocity, k is the light wavenumber in the diffractive section, and κ is the attenuation factor taking into account losses due to output coupling as well as distributed linear losses of the intracavity media.

Light propagation through the thin spectral filtering section is described by

$$A_1(t,x,y) = \int_{-\infty}^{t} f(t-\theta)A_3(\theta,x,y)\,\mathrm{d}\theta. \tag{2.3}$$

In particular, for a Lorentzian spectral filter with halfwidth γ and detuning ω_0, we choose $f(t) = \gamma\, \mathrm{e}^{(-\gamma+\mathrm{i}\omega_0)t}$.

Finally substituting (2.1) and (2.2) into (2.3), differentiating the resulting equation, and setting $\omega_0 = 0$ we obtain the following set of NDDEs:

$$\frac{\mathrm{d}A}{\mathrm{d}t} + \gamma A = \gamma\sqrt{\kappa}\,\frac{\mathrm{e}^{\mathrm{i}\phi}}{2\pi\,\mathrm{i}} \iint_{-\infty}^{\infty} \mathrm{e}^{\mathrm{i}((x-x')^2+(y-y')^2)/2} \times \mathrm{e}^{(1-\mathrm{i}\alpha_g)G/2-(1-\mathrm{i}\alpha_q)Q/2} A(t-T,x',y')\,\mathrm{d}x'\,\mathrm{d}y', \tag{2.4}$$

where $A(t,x,y) \equiv A_1(t,x,y)$, T is the total cold cavity round trip time, the propagation factor $\mathrm{i}kL$ has been absorbed into the phase ϕ, $\phi = \phi_1 + kL$, and saturable gain G and loss Q satisfy the equations [10–12]:

$$\frac{\mathrm{d}G}{\mathrm{d}t} = \gamma_{\mathrm{g}}(G_0 - G) - (e^G - 1)e^{-Q}|A(t-T,x,y)|^2 \tag{2.5}$$

and

$$\frac{\mathrm{d}Q}{\mathrm{d}t} = \gamma_q(Q_0 - Q) - s(1 - e^{-Q})|A(t-T,x,y)|^2. \tag{2.6}$$

Here, G_0 (Q_0) is the unsaturated gain (loss) parameter, γ_{g} (γ_q) is the carrier relaxation rate in the gain (absorber) section, and the parameter s is the ratio of saturation intensities in the gain and absorber sections. In the case of single transverse dimension instead of equation (2.4), we have

$$\frac{\mathrm{d}A}{\mathrm{d}t} + \gamma A = \gamma\sqrt{\kappa}\,\frac{\mathrm{e}^{\mathrm{i}\phi}}{\sqrt{2\pi\,\mathrm{i}}} \int_{-\infty}^{\infty} \mathrm{e}^{\mathrm{i}(x-x')^2/2}\,\mathrm{e}^{(1-\mathrm{i}\alpha_g)G/2-(1-\mathrm{i}\alpha_q)Q/2} A(t-T,x')\,\mathrm{d}x'. \tag{2.7}$$

NDDE models given by equations (2.4)–(2.6) and (2.5)–(2.7) can be considered as generalizations of the DDE model introduced in [10–12] to the case when the transverse diffraction of the laser beam is taken into account. In the next sections, we use these models for numerical study of LBs in a wide-aperture semiconductor mode-locked laser.

3. Simulations

(a) Numerical method

For numerical solution of equations (2.4)–(2.6) and (2.5)–(2.7), we perform Fourier transform (denoted by $\mathcal{F}_\perp$) of equations (2.4) (or (2.7)) in the transverse plane

$$\frac{\mathrm{d}\tilde{A}}{\mathrm{d}t} + \gamma\tilde{A} = \gamma\sqrt{\kappa}\,\mathrm{e}^{-\mathrm{i}q^2}\,\mathcal{F}_\perp[\mathrm{e}^{(1-\mathrm{i}\alpha_g)G/2-(1-\mathrm{i}\alpha_q)Q/2+\mathrm{i}\phi} A(t-T,x,y)], \tag{3.1}$$

with $\tilde{A} = \mathcal{F}_\perp[A]$, $q^2 = q_x^2 + q_y^2$ for system (2.4)–(2.6), and $q^2 = q_x^2$ for system (2.5)–(2.7). Here q_x and q_y are two components of the normalized transverse wavenumber. Note that for the sake of convenience in our numerical simulations starting from equation (3.1), we use the rescaled transverse variables $\bar{x} = x\sqrt{2}$ and $\bar{y} = y\sqrt{2}$, with overbar omitted. The numerical method is realized very similar to the conventional split-step method, so that systems (2.4)–(2.6) and (2.5)–(2.7) require as much computational effort as, e.g., $1+1$D and $2+1$D Ginzburg–Landau-type problems with delay, respectively [32–35]. First, using the delayed field $A(t-T,x,y)$, we obtain the values of G and Q on the next step by solving numerically equations (2.5) and (2.6). Second, we propagate the Fourier-transformed field $\tilde{A}$ one time-step further. Then the procedure is repeated. The large delay does not induce additional computational costs, because we use the values of the field that were calculated in the past. However, it increases significantly the memory requirements. These requirements could be, in principle, relaxed if we use the localized nature of our solution and store the delayed field $A(t-T,x,y)$ only when its absolute value is sufficiently large. Moreover, as it is shown in the following subsection, it is also possible to neglect completely the dynamics outside of a narrow temporal window around a single LB in a similar way as it was done for the MF models discussed in [8].

(b) Spectral method optimized for single light bullets

The field equation given by equation (2.4) can be formally rewritten as

$$\frac{\dot{A}}{\gamma} = -A + \hat{g}[A(t-T)], \tag{3.2}$$

where $\hat{g}$ is the nonlinear operator that combines the effect of gain, losses, diffraction and whose expression is given by the right-hand side of equation (2.4). Writing equation (3.2) in this particular form makes it apparent that the term $\hat{g}[A(t-T)]$ is a known nonlinear function of the field at the previous round trip. One can then solve equation (3.2) for the field profile over a whole round trip that we denote A_n. Several methods are possible, but the most convenient choice is to use the Fourier transform, since transverse diffraction can also be evaluated that way. In particular, the fact that the pulse train is asymptotic to zero makes it possible to apply the Fourier transform along the propagation axis (i.e. in the time domain) with periodic boundary conditions. Solving equation (3.2) in Fourier space and transforming back to the time domain yields a simple expression of the mapping operator

$$A_n = \mathcal{F}_t^{-1}\{\mathcal{L}(\omega)\mathcal{F}_t[\hat{g}(A_{n-1})]\}, \tag{3.3}$$

where $\mathcal{F}_t$ denotes the Fourier transform in time and $\mathcal{L}(\omega) = (1 + \mathrm{i}\omega/\gamma)^{-1}$ is the Lorentzian function. The fact that equations of the same type as equation (3.2) could be solved by a Fourier method as a functional mapping in the long delay limit was already pointed out in [36] for the case of a single variable. Applying Fourier transformation in the transverse plane yields the following form of the functional mapping:

$$A_n = \mathcal{F}_t^{-1}\{\mathcal{L}(\omega)\mathcal{F}_t\mathcal{F}_\perp^{-1}[\mathrm{e}^{-\mathrm{i}q^2}\mathcal{F}_\perp(\mathrm{e}^{(1-\mathrm{i}\alpha_g)G_{n-1}/2-(1-\mathrm{i}\alpha_q)Q_{n-1}/2+\mathrm{i}\phi}A_{n-1})]\}, \tag{3.4}$$

with the carrier profiles G_{n-1} and Q_{n-1} that can be deduced from the field distribution A_{n-1}. Finally, using the fact that the function $\mathcal{L}(\omega)$ $(\mathrm{e}^{-\mathrm{i}q^2})$ does not depend on transverse wavenumber q (frequency ω), we can reorder the Fourier transformations to obtain

$$A_n = \mathcal{F}^{-1}[\mathcal{U}(\omega,q)\mathcal{F}(\mathrm{e}^{(1-\mathrm{i}\alpha_g)G_{n-1}/2-(1-\mathrm{i}\alpha_q)Q_{n-1}/2+\mathrm{i}\phi}A_{n-1})], \tag{3.5}$$

with $\mathcal{F} = \mathcal{F}_t \circ \mathcal{F}_\perp$ and $\mathcal{U}(\omega,q) = \mathcal{L}(\omega)\,\mathrm{e}^{-\mathrm{i}q^2}\exp(-\mathrm{i}\upsilon\omega)$, where the last exponential factor represents an ad hoc correction to the natural drift of the temporal solution from one round trip towards the next. Such drift is found in most DDE systems and in our case one can simply take $\upsilon \approx -1/\gamma$, see [11,36] for more details.

A numerical method based on the use of equation (3.5) was applied to calculate bifurcation diagrams of the LB solutions. An important advantage of this approach is that the temporal domain along the t-axis can be taken much smaller than the delay time T, e.g. a few times larger than the LB temporal width, yielding a considerable reduction of computational cost; see [37] for more details on this functional mapping approach.

4. Results

(a) Light bullets in the mean-field approximation

Self-organization mechanism leading to the formation of LBs in the wide-aperture mode-locked laser is related to the presence of saturable absorption in the laser cavity rather than self-focusing Kerr nonlinearity, and one can observe them with zero alpha-factors [8]. Therefore, we start with the simplest case $\alpha_g = \alpha_q = 0$ and choose the parameter region, where the gain and loss per cavity round trip are relatively small, so that the MF approximation can be used: $\kappa = 0.8$, $Q_0 = 0.3$, $\gamma_\mathrm{g} = 0.04$, $\gamma_q = 1.0$, $s = 30$, $\gamma = 40$, $T = 200$. We vary the normalized gain $g_0 = G_0/g_\mathrm{th}$, where $g_\mathrm{th} = Q_0 - \log\kappa$, below the lasing threshold $g_0 < 1$.

A stable two-dimensional LB calculated for $g_0 = 0.68$ is shown in figure 2, while figure 3 presents a stable three-dimensional LB obtained for $g_0 = 0.69$. Note that the very long tail of the

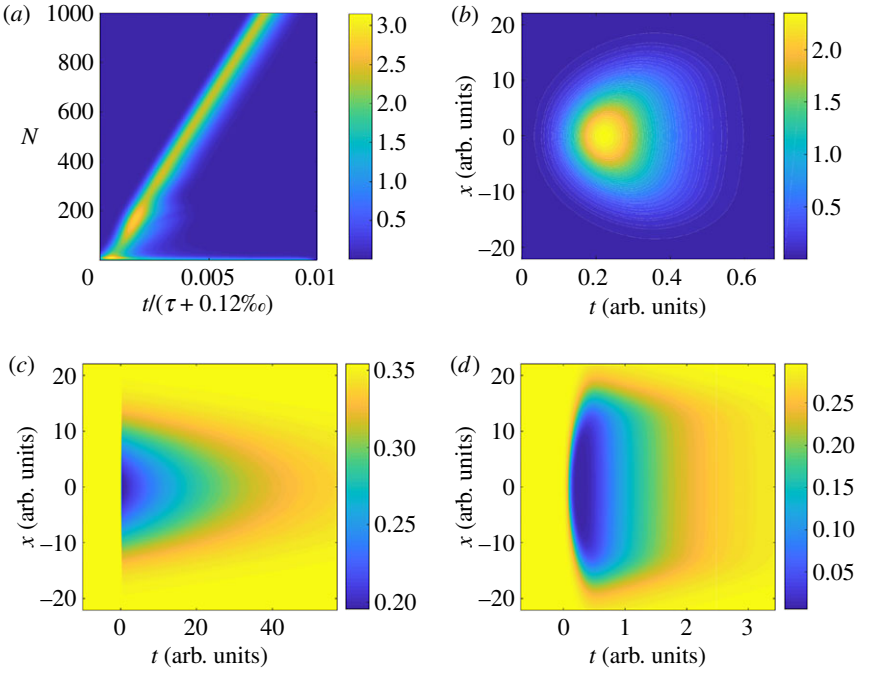

Figure 2. Two-dimensional LB solution obtained by the numerical integration of equations (2.5)–(2.7) for $g_0 = 0.68$. (*a*) The space–time representation of the maximal intensity $\max_x |A(t,x)|^2$, where N is the number of round trips adjusted by a multiplication factor 1.00012, which reduces the speed of the LB and improves its visibility in the representation. Panels (*b*), (*c*) and (*d*) show spatio-temporal profiles of LB intensity $|A(t,x)|^2$, saturable gain $G(t,x)$ and saturable loss $Q(t,x)$, respectively. Other parameters are $\kappa = 0.8$, $Q_0 = 0.3$, $\gamma_g = 0.04$, $\gamma_q = 1.0$, $s = 30$, $\gamma = 40$, $T = 200$, $\alpha_g = \alpha_q = 0$. (Online version in colour.)

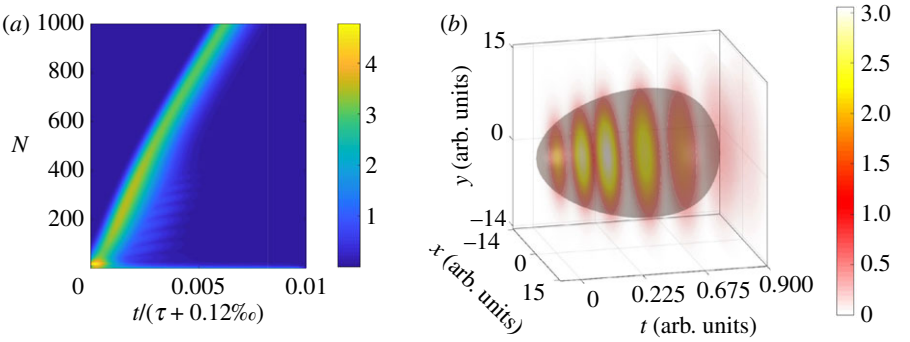

Figure 3. Three-dimensional LB obtained by numerical solution of equations (2.4)–(2.6) for $g_0 = 0.69$. Panel (*a*) demonstrates the space–time representation of the maximal intensity $\max_{x,y} |A(t,x,y)|^2$, whereas (*b*) shows a spatio-temporal profile of the LB intensity $|A(t,x,y)|^2$. Other parameters are as in figure 2. (Online version in colour.)

LB that stems from the slow gain profile is fully resolved by solving numerically equations (2.4)–(2.6) (or (2.5)–(2.7)). Unlike the Haus-type model, which was used earlier in [8] for qualitative modelling of LB regime in the MF limit, these equations give a more realistic description of dynamical behaviour of a wide aperture mode-locked semiconductor laser under investigation. Therefore, our results presented in figures 2 and 3 provide further arguments in favour of the feasibility of the experimental observation of LBs, predicted in the earlier works [8,9].

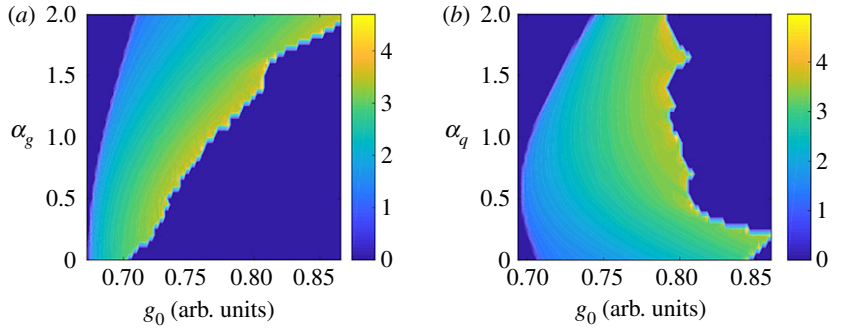

Figure 4. Domains of the existence of stable two-dimensional LBs calculated by numerical integration of equations (2.5)–(2.7). Panel *a* (*b*) is obtained by varying the parameters g_0 and α_g (α_q) with fixed $\alpha_q = 0.5$ ($\alpha_g = 1.5$). Other parameters are as in figure 2. The colour code represents the peak intensity of the LB pulse. (Online version in colour.)

The domains of the existence of stable two-dimensional LBs obtained by numerical integration of equations (2.5)–(2.7) are shown in figure 4. Figure 4*a* (figure 4*b*) presents the stability domain in the plane of two parameters, pump parameter g_0 and linewidth enhancement factor α_g (α_q) in the gain (absorber) section of the laser. The parameter scans were performed by taking a stable LB calculated at fixed values of the linewidth enhancement factors $\alpha_g = 1.5$ and $\alpha_q = 0.5$ as an initial condition, and then performing numerical continuation of the LB branch by increasing and decreasing g_0. For each value of g_0, $N = 100$ round trips in the laser cavity were calculated. After that we calculate the centre of the stability range in g_0, pick the corresponding LB as an initial condition, make a small step in the linewidth enhancement factor and repeat the above-described procedure. It is noteworthy that the stability domains shown in figure 4 are in good qualitative agreement with those obtained in [9] using the Haus-type model (see figure 9 and the discussion in §4c). It can be seen from this figure that moderate non-zero linewidth enhancement factors can enlarge the LB stability range. The main difference of the results presented here with those obtained using the Haus-type model is that in the NDDE system (2.5)–(2.7) predicts slightly larger stability domains of LBs. We suggest that this discrepancy may be attributed to finite size of the integration interval, different continuation procedures, as well as to the use of different models. Note that the lack of quantitative agreement between the results reported in [9] (figure 9) with the bifurcation diagrams shown in figure 4 may indicate that future studies could profit from the use of NDDE models even in the parameter domain where MF Haus-type mode-locking models were successfully applied earlier for qualitative analysis of the LB formation [8,9]. More detailed comparison of the two models requires further studies.

(b) Light bullets beyond the mean field approximation

In the previous subsection, we demonstrated that in the MF limit the results obtained with the NDDE models (2.4)–(2.7) are in a very good agreement with those from the Haus-type model used in [8,9], and pointed out some minor discrepancies between the two models. In this subsection, we use the NDDE model to investigate how the properties of LBs are modified away from the MF limit. To this end, we consider relatively large gain and loss per cavity round trip time, which is typical of semiconductor lasers: $\kappa = 0.3$, $Q_0 = 2.0$, $\gamma_g = 0.04$, $\gamma_q = 1.0$, $s = 30$, $\gamma = 10$, $T = 200$, $\alpha_g = 1.5$, $\alpha_q = 0.5$. A stable two-dimensional LB obtained by numerical integration of equations (2.5)–(2.7) with $g_0 = 0.83$ is presented in figure 5. Using a two-parameter scan similar to that described in the previous subsection, we find even larger parameter domains of the existence of stable LBs than those obtained in the case of relatively small gain and loss; compare figure 6 with figure 4. Note, that when the difference $\alpha_g - \alpha_q$ becomes sufficiently large (between 1.5 and 2, see, for example, the region $0 \leq \alpha_q \leq 0.2$ in figure 6*b*), a sufficiently good initial guess is required to ensure

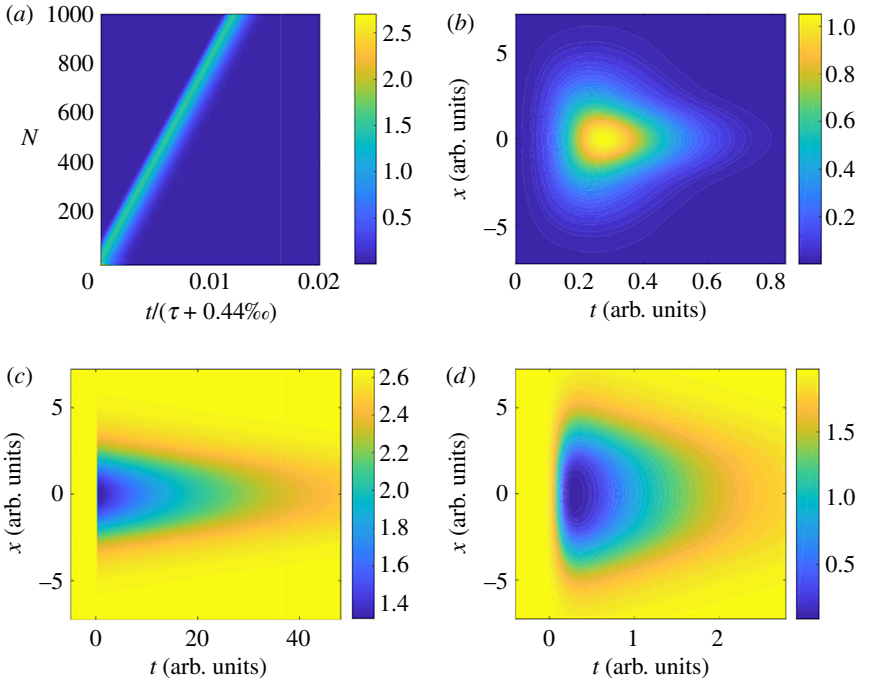

Figure 5. Two-dimensional LB obtained by the numerical integration of equations (2.5)–(2.7) for $g_0 = 0.83$. Panel (*a*) demonstrates space–time representation of the maximal intensity $\max_x |A(t,x)|^2$. Panels (*b*), (*c*) and (*d*) show spatio-temporal profiles of the LB intensity $|A(t,x)|^2$, saturable gain $G(t,x)$ and saturable absorption $Q(t,x)$, respectively. Other parameters are: $\kappa = 0.3, q_0 = 2.0, \gamma_g = 0.04, \gamma_q = 1.0, s = 30, \gamma = 10, T = 200, \alpha_g = 1.5, \alpha_q = 0.5$. (Online version in colour.)

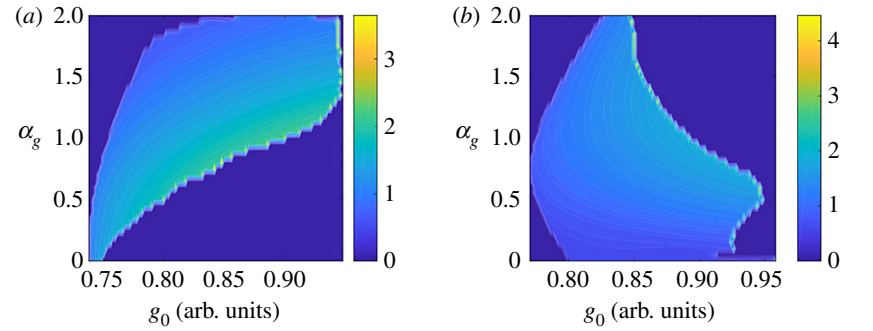

Figure 6. Domains of existence of stable LBs obtained by numerical integration of equations (2.5)–(2.7). Panel *a* (*b*) panel is obtained by varying two parameters g_0 and α_g (α_q) with fixed $\alpha_q = 0.5$ ($\alpha_g = 1.5$). Other parameters are as in figure 5. The colour code represents the peak intensity of the LB pulse. (Online version in colour.)

a convergence of the solution to a stable LB. Finally, figure 7 shows an example of stable three-dimensional LB obtained by solving equations (2.4)–(2.6) with $g_0 = 0.92$.

(c) Spectral method

As we have already mentioned above, the application of spectral method based on the functional mapping described in §3b allows us to calculate the LB solution on a time interval much shorter than the cavity round trip time T and, hence, to reduce considerably the amount of calculations.

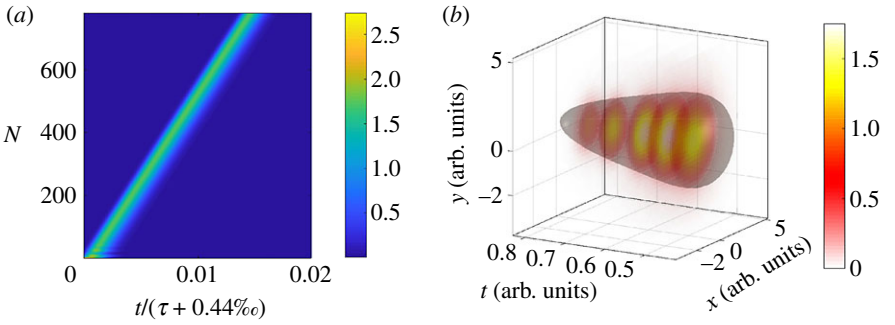

Figure 7. Three-dimensional LB obtained by the numerical solution of equations (2.4)–(2.6) for $g_0 = 0.92$. Other parameters are as in figure 5. Panel (*a*) demonstrates space–time representation of the maximal intensity $\max_x |A(t, x, y)|^2$. Panel (*b*) shows spatio-temporal profile of the LB intensity $|A(t, x, y)|^2$. (Online version in colour.)

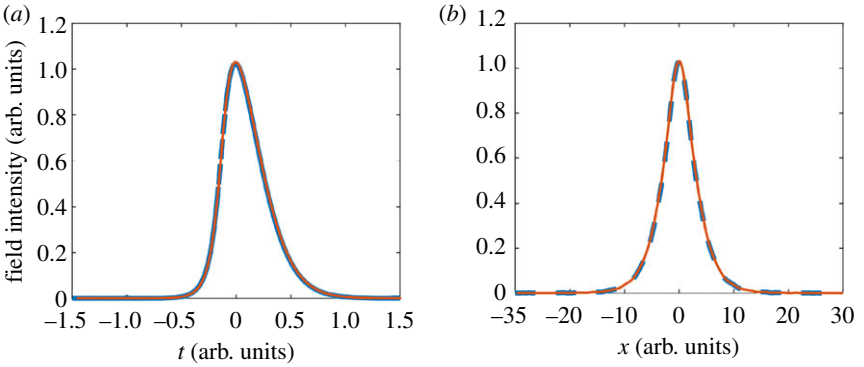

Figure 8. Longitudinal (*a*) and transverse (*b*) intensity profiles of two-dimensional LBs obtained by direct numerical integration of equations (2.5)–(2.7) and using the functional mapping (3.5) are shown by dashed line and solid line, respectively. Parameters are the same as in figure 5. (Online version in colour.)

Transverse and longitudinal profiles of a two-dimensional LB solution calculated with the help of the optimized spectral method given by equation (3.5) are presented in figure 8 together with the profiles obtained by direct numerical solution of the NDDE model (2.5)–(2.7) using the method described in §3a. One can see that the agreement between the results obtained with two different numerical approaches is almost perfect. Similarly, the stability domains of an LB solution calculated with the help of the functional mapping method and shown in figure 9 are in a good agreement with those presented in figure 6. Small discrepancies in the two-parameter stability diagrams can be explained by differences in the numerical continuation procedure. In particular, the continuation of the LB solution can be performed only with a good initial guess, which we accomplished as described in the previous subsection. On the other hand, numerical simulations of the mapping procedure (3.5) are very fast, and it is more efficient to perform two-parameter scans by finding a stable LB solution for each value of the linewidth enhancement factor and then continuing it in g_0. It is seen from figure 9 that the latter approach fails to find a stable LB around $\alpha_g \approx 2$ (figure 9*a*) and $\alpha_q \approx 0.2$ (figure 9*b*), whereas a slower continuation approach based on direct numerical integration of equations (2.5)–(2.7) indicates that stable LBs exist in these parameter domains (cf. figure 6). This discrepancy is related to the fact that at large differences $\alpha_g - \alpha_q$ it is hardly possible to excite stable LBs from an arbitrary initial condition not only by using the functional mapping method, but also by solving numerically the NDDE system on the full round trip time interval.

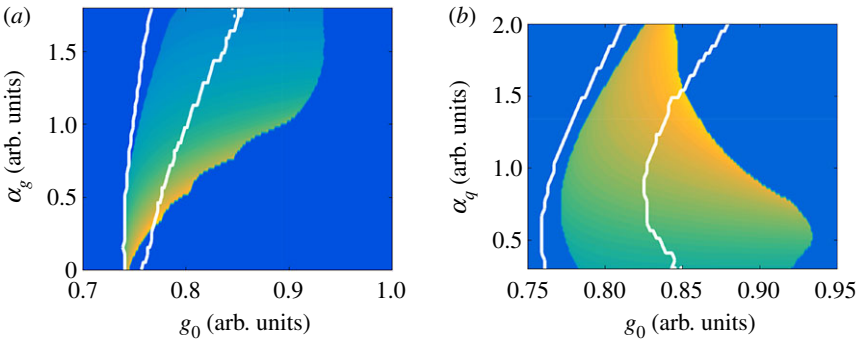

Figure 9. Domains of existence of stable two-dimensional LBs obtained with the help of the functional mapping (3.5). Panel *a* (*b*) is obtained by varying the parameters g_0 and α_g (α_q) with fixed $\alpha_q = 0.5$ ($\alpha_g = 1.5$). Other parameters are as in figure 5. Colour code represents the energy of the pulse, $\iint |A(t,x)|^2\, dx\, dt$. White lines represent stability domain borders of the LBs calculated using the Haus model [9], which are shifted to higher current with an offset $\delta g = 0.06$. (Online version in colour.)

To continue the discussion about the validity of the MF approximation started in §4a, in figure 9 we superpose the results from the NDDE model (2.5)–(2.7) with exponential gain and absorption with those of the Haus equation model (cf. [9]) shifted to higher currents with an offset $\delta g = 0.06$. One can see that both models predict the existence of LBs with almost the same parameters, similar stability ranges and similar dependence of these ranges on the α-factors in the gain and absorber sections: a moderate increase of $\alpha_g - \alpha_q$ ($\alpha_g \geq \alpha_q$) leads to an increase of the LB stability range. However, the quantitative agreement is not that good. Notwithstanding the offset δg of approximately 8% to higher currents in figure 9, some salient differences remain, in particular for large values of α_g and α_q. While the detailed investigation of these differences is out of scope of this paper, in what follows we will identify three main sources of the discrepancies.

First, the linearization of the gain and absorption in the Haus model [9] accounts for a part of the quantitative disagreement. The values of the unsaturated loss parameter in the absorber section, $Q_0 = 0.3$, and linear round trip loss per cavity round trip, $\kappa - 1 = 0.2$, used in [9], are relatively small quantities, but they are not infinitesimal. For instance, the discrepancy between the lasing threshold in [9] defined by $g_{\mathrm{th}}^{l} = 2(\kappa^{-1/2} - 1) + Q_0 \approx 0.536$ and the threshold obtained with the NDDE model (2.5)–(2.7), $g_{\mathrm{th}} = -\ln\kappa + Q_0 \approx 0.523$, is evaluated to approximately 2.5%. Therefore, other thresholds such as saddle-node bifurcations of the LBs are also bound to shift slightly in g_0 due to the difference between the linear and exponential gain.

Secondly, the NDDE model (2.5)–(2.7) can be transformed into a partial differential Haus-type equation [9] with the help of the multiple time-scale analysis, where a 'spatial' operator acting on the fast time scale replaces the delay operator [29,36]. This can only be done by neglecting higher order derivatives (beyond diffusion) along the longitudinal direction. This approximation results in a discrepancy between the models for almost all parameter values.

Finally, the NDDE model (2.5)–(2.7) accounts for diffraction via a lumped exponential operator $\exp(\mathrm{i}q^2)$ (in Fourier domain), whereas the Haus model [9] considers an additive operator $\mathrm{i}q^2$. Therefore, these approaches might yield identical results only for long wavelength LSs, for which the characteristic wavelength $\lambda_c \gg 1$ so that $\exp(\mathrm{i}q^2) \approx 1 + \mathrm{i}q^2$. In our case, the typical FWHM of the LBs in the transverse dimension is $\lambda_c \sim 6$ (cf. figure 8*b*), which is not particularly large and can explain some of the differences between the two approaches. In our case, the qualitative convergence between the two models stems from the fact that in the MF regime ($Q_0 \to 0, G_0 \to 0, \kappa \to 1$) the LBs become wider in the transverse dimension.

After we have demonstrated the quantitative accuracy of the functional mapping (3.5), we can use it to investigate the effect of large losses on the LB stability domain. Figure 10 illustrates how the stability domain on the plane of two parameters, normalized unsaturated gain g_0, and normalized unsaturated loss $q_0 = Q_0/-\log\kappa$, changes with the decrease of the linear attenuation

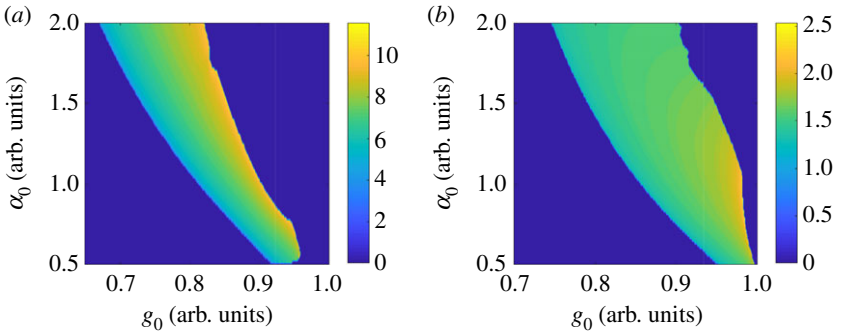

Figure 10. Domains of existence of stable LBs on the plane of two parameters, g_0 and $q_0 = Q_0/-\log\kappa$, obtained with the help of the functional mapping (3.5). Panel *a* (*b*) corresponds to $\kappa = 0.8$ ($\kappa = 0.3$). Other parameters are as in figure 5. Colour code represents the energy of the pulse. (Online version in colour.)

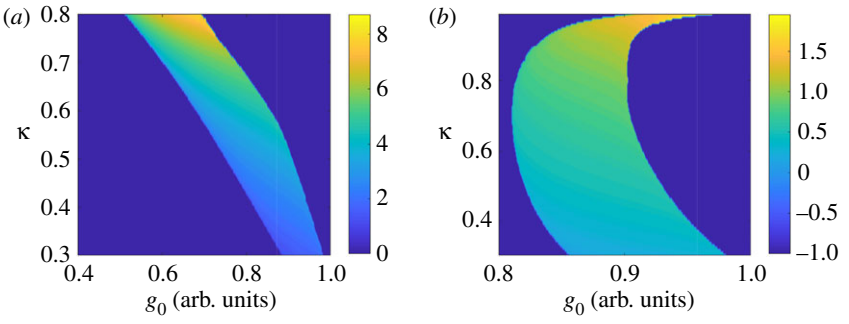

Figure 11. Domains of existence of stable LBs obtained with the help of the functional mapping (3.5) by varying the parameters g_0 and κ with fixed $Q_0 = 1$ (*a*) and with varying $Q_0 = -\log\kappa$ (i.e. fixed $q_0 = 1$) (*b*). Other parameters are as in figure 5. Colour code represents the energy of the pulse. (Online version in colour.)

factor κ, i.e. with the increase of the linear cavity losses. Note that similar bifurcation diagram reported in [9] for the case small losses, $\kappa = 0.8$, is qualitatively similar to that shown in figure 10. It follows also from this figure that the LB stability range increases with the absolute value of the unsaturated loss parameter. The LB stability domains on the plane of two parameters, normalized pump parameter g_0, and attenuation factor κ, are shown in figure 11*a* corresponding to fixed value of the unsaturated absorption parameter $Q_0 = 1$. According to this figure the increase of linear losses results in a slight decrease of the LS stability range. Finally, by decreasing κ and increasing Q_0 so that $q_0 = Q_0/-\log\kappa = 1$ is constant, we see from figure 11*b* that the decrease of the LS stability range due to increased losses can be compensated by increasing the unsaturated loss parameter. Furthermore, by increasing κ up to 0.99 and decreasing Q_0 simultaneously we see that the LB broadens in all dimensions, and in the regime, when the linear and saturable losses are small enough and the length of the LB becomes larger than the absorber recovery time, $\gamma_q^{-1} = 1$, we observe that the LB stability range in g_0 shrinks fast to the point $g_0 = \kappa = 1$ corresponding to the MF limit with a fast absorber.

5. Conclusion

We have proposed an NDDE model of a wide-aperture mode-locked laser and used this model to demonstrate the existence of stable LBs in a semiconductor lasers, where the small gain and loss approximation is usually not justified. Unlike the Haus-type model, which was used previously

to predict the existence of LBs and explain the mechanism of their formation theoretically [8,9], the NDDE model is not based on the MF approximation. We have shown that, although in the MF approximation the qualitative agreement between the results obtained using these two models is very good, for the parameter region studied in [8,9] the Haus-type model is already rather close to the limits of its applicability. Therefore, even in this parameter region the NDDE model can provide a more accurate description of the LBs stability domain. A detailed investigation of an interesting question, how far the agreement between NDDE and Haus-type models regarding the existence and the stability properties of the LBs stands, could be a subject of further studies. For example, it is known that the Q-switching instability of the mode-locked regime is well described by the DDE model, but can be missing in Haus-type models [29]. Moving away from the MF approximation we have demonstrated the existence of LBs in a laser with relatively large gain and losses per cavity round trip. We have found that the increase of the absolute value of the unsaturated loss parameter can lead to an increase of the stability range of LBs, and, in particular, to a compensation of the destabilizing effect of large linear losses. Thus, our results provide further guidelines for future experimental observation of LBs in mode-locked semiconductor lasers.

Data accessibility. This article has no additional data.

Authors' contributions. A.G.V. proposed the delay integro-differential model and derived it together with A.P. S.G. and J.J. developed the functional mapping method for its solution. A.P., S.G. and J.J. developed the software for the numerical simulations. A.P. carried out the numerical simulations. All authors equally participated in the design of the study, interpretation of the numerical results, and preparation and approval of the manuscript.

Competing interests. We declare we have no competing interests.

Funding. A.P. and A.G.V. acknowledge the support of the SFB 787 of the DFG, project B5. A.G.V. acknowledges the support grant no. 14-41-00044 of the Russian Science Foundation. J.J. acknowledges financial support project COMBINA (TEC2015-65212-C3-3-P AEI/FEDER UE). S.G. acknowledges the Universitat de les Illes Balears for funding a stay where part of this work was developed.

Acknowledgements. The authors thank Sh. Amiranashvili for useful discussions on the topic.

References

1. Akhmediev N, Ankiewicz A 2008 *Dissipative solitons: from optics to Biology and medicine*. Lecture Notes in Physics, vol. 751. Berlin, Germany: Springer.
2. Silberberg Y. 1990 Collapse of optical pulses. *Opt. Lett.* **15**, 1282–1284. (doi:10.1364/OL.15.001282)
3. Zakharov VE. 1972 Collapse of Langmuir waves. *Soviet Phys. JETP* **35**, 908–914.
4. Rasmussen JJ, Rypdal K. 1986 Blow-up in nonlinear Schroedinger equations-I. A general review. *Physica Scripta* **33**, 481–497. (doi:10.1088/0031-8949/33/6/001)
5. Veretenov N, Tlidi M. 2009 Dissipative light bullets in an optical parametric oscillator. *Phys. Rev. A* **80**, 023822. (doi:10.1103/PhysRevA.80.023822)
6. Veretenov N, Vladimirov A, Kaliteevskii N, Rozanov N, Fedorov S, Shatsev A. 2000 Conditions for the existence of laser bullets. *Opt. Spectrosc.* **89**, 380–383. (doi:10.1134/1.1310704)
7. Brambilla M, Maggipinto T, Patera G, Columbo L. 2004 Cavity light bullets: three-dimensional localized structures in a nonlinear optical resonator. *Phys. Rev. Lett.* **93**, 203901. (doi:10.1103/PhysRevLett.93.203901)
8. Javaloyes J. 2016 Cavity light bullets in passively mode-locked semiconductor lasers. *Phys. Rev. Lett.* **116**, 043901. (doi:10.1103/PhysRevLett.116.043901)
9. Gurevich SV, Javaloyes J. 2017 Spatial instabilities of light bullets in passively-mode-locked lasers. *Phys. Rev. A* **96**, 023821. (doi:10.1103/PhysRevA.96.023821)
10. Vladimirov AG, Turaev D. 2004 New model for mode-locking in semiconductor lasers. *Radiophys. Quantum Electron.* **47**, 857–865.
11. Vladimirov AG, Turaev D. 2005 Model for passive mode-locking in semiconductor lasers. *Phys. Rev. A* **72**, 033808 (13 pages). (doi:10.1103/PhysRevA.72.033808)

12. Vladimirov A, Turaev D, Kozyreff G. 2004 Delay differential equations for mode-locked semiconductor lasers. *Opt. Lett.* **29**, 1221–1223. (doi:10.1364/OL.29.001221)
13. Marconi M, Javaloyes J, Balle S, Giudici M. 2014 How lasing localized structures evolve out of passive mode locking. *Phys. Rev. Lett.* **112**, 223901. (doi:10.1103/PhysRevLett.112.223901)
14. Puzyrev D, Vladimirov AG, Pimenov A, Gurevich SV, Yanchuk S. 2017 Bound pulse trains in arrays of coupled spatially extended dynamical systems. *Phys. Rev. Lett.* **119**, 163901. (doi:10.1103/PhysRevLett.119.163901)
15. Heuck M, Blaaberg S, Mørk J. 2010 Theory of passively mode-locked photonic crystal semiconductor lasers. *Opt. Express* **18**, 18003–18014. (doi:10.1364/OE.18.018003)
16. Pimenov A, Tronciu VZ, Bandelow U, Vladimirov AG. 2013 Dynamical regimes of a multistripe laser array with external off-axis feedback. *J. Opt. Soc. Am. B* **30**, 1606–1613. (doi:10.1364/JOSAB.30.001606)
17. Slepneva S, Kelleher B, O'Shaughnessy B, Hegarty S, Vladimirov AG, Huyet G. 2013 Dynamics of fourier domain mode-locked lasers. *Opt. Express* **21**, 19 240–19 251. (doi:10.1364/OE.21.019240)
18. Slepneva S, O'Shaughnessy B, Kelleher B, Hegarty S, Vladimirov AG, Lyu H, Karnowski K, Wojtkowski M, Huyet G. 2014 Dynamics of a short cavity swept source oct laser. *Opt. Express* **22**, 18 177–18 185. (doi:10.1364/OE.22.018177)
19. Jaurigue L, Pimenov A, Rachinskii D, Schöll E, Lüdge K, Vladimirov AG. 2015 Timing jitter of passively-mode-locked semiconductor lasers subject to optical feedback: a semi-analytic approach. *Phys. Rev. A* **92**, 053807. (doi:10.1103/PhysRevA.92.053807)
20. Rebrova N, Huyet G, Rachinskii D, Vladimirov AG. 2011 Optically injected mode-locked laser. *Phys. Rev. E* **83**, 066202. (doi:10.1103/PhysRevE.83.066202)
21. Arkhipov R, Pimenov A, Radziunas M, Rachinskii D, Vladimirov AG, Arsenijevic D, Schmeckebier H, Bimberg D. 2013 Hybrid mode-locking in semiconductor lasers: simulations, analysis and experiments. *IEEE J. Sel. Top. QE* **99**, 1100208. (doi:10.1109/JSTQE.2012.2228633)
22. Pimenov A, Viktorov EA, Hegarty SP, Habruseva T, Huyet G, Rachinskii D, Vladimirov AG. 2014 Bistability and hysteresis in an optically injected two-section semiconductor laser. *Phys. Rev. E* **89**, 052903. (doi:10.1103/PhysRevE.89.052903)
23. Arkhipov RM, Habruseva T, Pimenov A, Radziunas M, Hegarty SP, Huyet G, Vladimirov AG. 2016 Semiconductor mode-locked lasers with coherent dual-mode optical injection: simulations, analysis, and experiment. *J. Opt. Soc. Am. B* **33**, 351–359. (doi:10.1364/JOSAB.33.000351)
24. Wong YL, Carroll JE. 1987 A travelling-wave rate equation analysis for semiconductor lasers. *Solid-State Electron.* **30**, 13–19. (doi:10.1016/0038-1101(87)90024-4)
25. Bandelow U, Radziunas M, Sieber J, Wolfrum M. 2001 Impact of gain dispersion on the spatio-temporal dynamics of multisection lasers. *IEEE J. Quantum Electron.* **37**, 183–188. (doi:10.1109/3.903067)
26. Bandelow U, Radziunas M, Vladimirov A, Huettl B, Kaiser R. 2006 40 GHz modelocked semiconductor lasers: theory, simulations and experiment. *Opt. Quantum Electron.* **38**, 495–512. (doi:10.1007/s11082-006-0045-2)
27. Javaloyes J, Balle S. 2010 Mode-locking in semiconductor fabry-perot lasers. *IEEE J. Quantum Electron.* **46**, 1023–1030. (doi:10.1109/JQE.2010.2042792)
28. Javaloyes J, Balle S. 2010 Quasiequilibrium time-domain susceptibility of semiconductor quantum wells. *Phys. Rev. A* **81**, 062505. (doi:10.1103/PhysRevA.81.062505)
29. Kolokolnikov T, Nizette M, Erneux T, Joly N, Bielawski S. 2006 The Q-switching instability in passively mode-locked lasers. *Phys. D: Nonlinear Phenom.* **219**, 13–21. (doi:10.1016/j.physd.2006.05.006)
30. Vladimirov AG, Huyet G, Pimenov A. 2016 Delay differential models in multimode laser dynamics: taking chromatic dispersion into account. *Proc. SPIE* **9892**, 98920I–98920I–7. (doi:10.1117/12.2230649)
31. Pimenov A, Slepneva S, Huyet G, Vladimirov AG. 2017 Dispersive time-delay dynamical systems. *Phys. Rev. Lett.* **118**, 193901. (doi:10.1103/PhysRevLett.118.193901)
32. Tlidi M, Vladimirov A, Pieroux D, Turaev D. 2009 Spontaneous motion of cavity solitons induced by a delayed feedback. *Phys. Rev. Lett.* **103**, 103904. (doi:10.1103/PhysRevLett.103.103904)

33. Panajotov K, Tlidi M. 2010 Spontaneous motion of cavity solitons in vertical-cavity lasers subject to optical injection and to delayed feedback. *Eur. Phys. J. D-Atomic, Mol. Opt. Plasma Phys.* **59**, 67–72. (doi:10.1140/epjd/e2010-00111-y)
34. Pimenov A, Vladimirov AG, Gurevich SV, Panajotov K, Huyet G, Tlidi M. 2013 Delayed feedback control of self-mobile cavity solitons. *Phys. Rev. A* **88**, 053830. (doi:10.1103/PhysRevA.88.053830)
35. Puzyrev D, Yanchuk S, Vladimirov A, Gurevich S. 2014 Stability of plane wave solutions in complex Ginzburg–Landau equation with delayed feedback. *SIAM J. Appl. Dyn. Syst.* **13**, 986–1009. (doi:10.1137/130944643)
36. Giacomelli G, Politi A. 1996 Relationship between delayed and spatially extended dynamical systems. *Phys. Rev. Lett.* **76**, 2686–2689. (doi:10.1103/PhysRevLett.76.2686)
37. Schelte C, Javaloyes J, Gurevich SV. In press. Functional mapping for passively mode-locked semiconductor lasers. *Opt. Lett.*